# Pseudorapidity distributions of charged particles in asymmetric collisions using Tsallis thermodynamics*

J.Q. Tao,[1] H.B. He,[2] H. Zheng,[2,†] W.C. Zhang,[2] X. Liu,[3] L.L. Zhu,[4] and A. Bonasera[5,6]

[1]*Key Laboratory of Quark & Lepton Physics (MOE) and Institute of Particle Physics, Central China Normal University, Wuhan 430079, China*
[2]*School of Physics and Information Technology, Shaanxi Normal University, Xi'an 710119, China*
[3]*Institute of Nuclear Science and Technology, Sichuan University, Chengdu 610064, China*
[4]*Department of Physics, Sichuan University, Chengdu 610064, China*
[5]*Cyclotron Institute, Texas A&M University, College Station, TX 77843, USA*
[6]*Laboratori Nazionali del Sud, INFN, 95123 Catania, Italy*

The pseudo-rapidity distributions of the charged particles produced in the asymmetric collision systems p+Al, p+Au and $^3$He+Au at $\sqrt{s_{NN}} = 200$ GeV are evaluated in the framework of a fireball model with Tsallis thermodynamics. The fireball model assumes that the experimentally measured particles are produced by fireballs following the Tsallis distribution and it can effectively describe the experimental data. Our results as well as previous results for d+Au collisions at $\sqrt{s_{NN}} = 200$ GeV and p+Pb collisions at $\sqrt{s_{NN}} = 5.02$ TeV validate that the fireball model based on Tsallis thermodynamics can provide a universal framework for pseudo-rapidity distribution of the charged particles produced in asymmetric collision systems. We predict the centrality dependence of the total charged particle multiplicity in the p+Al, p+Au and $^3$He+Au collisions. Additionally, the dependences of the fireball model parameters ($y_{0a}$, $y_{0A}$, $\sigma_a$ and $\sigma_A$) on the centrality and system size are studied.

Keywords: Tsallis thermodynamics, Fireball model, Pseudo-rapidity distribution, Heavy-ion collisions, Charged particles



## I. INTRODUCTION

High-energy heavy-ion collisions provide a unique way to understand the origin of the universe. However, their processes cannot be directly observed in experiment. We can only study the collision process indirectly by analyzing the properties of the final particles produced in the collisions. The pseudo-rapidity distribution of charged particles is one of the important experimental observables. The study of this observable could lead to a better understanding of the properties of the particles produced in the collisions, the particle production mechanism and so on. There have been numerous works in previous studies using different models, such as HIJING [1], AMPT [2–4], EPOS-LHC [5], a multi-source thermal model [6, 7], a new revised Landau hydrodynamics model [8], a 1 + 1 dimensional hydrodynamics model [9, 10], a dynamical initial state model coupled to (3 + 1)D viscous relativistic hydrodynamics [11] and so on, to analyze the existing experimental data of pseudo-rapidity distributions of the charged particles [12–30]. Although these models are based on different physical ideas, valuable physical information on the collision process has been extracted and learned.

Recently, a fireball model based on Tsallis thermodynamics was utilized to analyze the pseudo-rapidity distribution of the charged particles measured in high-energy heavy-ion collisions [31–33]. In our previous works [32, 33], we used the fireball model to study the pseudo-rapidity distributions of the charged particles produced in p+p($\overline{\rm p}$) collisions for energies ranging from $\sqrt{s_{NN}}$ = 23.6 GeV to 13 TeV and A+A collisions at the RHIC and LHC, and extended the fireball model to the asymmetric collision systems, i.e., d+Au collisions at $\sqrt{s_{NN}} = 200$ GeV and p+Pb collisions at $\sqrt{s_{NN}} = 5.02$ TeV, by considering the asymmetric collision geometry configuration. In this paper, we utilize recently published data from the PHINEX Collaboration [30] at RHIC to systematically study the pseudo-rapidity distributions of the charged particles produced in asymmetric collision systems, including p+Al, p+Au and $^3$He+Au collisions at $\sqrt{s_{NN}} = 200$ GeV. We also predict the total multiplicities of the charged particles from the fireball model and study their centrality dependence. Further, we analyze the centrality and system size dependencies of the fireball model parameters obtained from the pseudo-rapidity distributions of the charged particles.

The paper is organized as follows. In section II, the fireball model with Tsallis thermodynamics is briefly introduced. In section III, the fitting results of the fireball model and the total charged particle multiplicities extracted from the fireball model are shown. The dependences of the model parameters on the centrality and size of the collision systems are also presented. A brief conclusion is drawn in section IV.

## II. THEORETICAL DESCRIPTIONS

In the self-consistent Tsallis thermodynamics, the Tsallis distribution is proposed as a generalization of the Boltzmann–Gibbs distribution [34]. To describe the transverse momentum spectrum of particles, the Tsallis distribution is writ-

* This work was supported in part by the National Natural Science Foundation of China under Grants No. 11905120, No. 11947416, by the Natural Science Foundation of Sichuan Province under Grant No. 2023NSFSC1322, by the Natural Science Basic Research Plan in Shaanxi Province of China under Grant No. 2023-JC-YB-012, by the United States Department of Energy under Grant # DE-FG02-93ER40773 and the NNSA Grant No. DENA0003841 (CENTAUR).

† Corresponding author, zhengh@snnu.edu.cn

ten as [31–33]

$$\frac{d^2N}{2\pi p_T dp_T dy} = gV\frac{m_T\cosh y}{(2\pi)^3} \times\left[1+(q-1)\frac{m_T\cosh y-\mu}{T}\right]^{-\frac{q}{q-1}}, \quad (1)$$

where $g$ is the particle state degeneracy, $V$ is the volume, $m_T=\sqrt{m_0^2+p_T^2}$ is the transverse mass and $m_0$ is the particle rest mass, $y$ is the rapidity, $q$ is the entropic factor, which measures the non-additivity of the entropy [34, 35], $\mu$ is the chemical potential and $T$ is the temperature. The Boltzmann distribution is recovered when $q=1$. We take $\mu=0$ because the multiplicities of $\pi^+$ and $\pi^-$ are equal and they are the majority of particles produced in the collision systems considered. For the middle rapidity $y\approx 0$, Eq. (1) can be rewritten as

$$\frac{d^2N}{2\pi p_T dp_T dy} = gV\frac{m_T}{(2\pi)^3}\left[1+(q-1)\frac{m_T}{T}\right]^{-\frac{q}{q-1}}. \quad (2)$$

The parameters $q$ and $T$ are extracted from the experimental transverse momentum spectrum of the particles.

In the fireball model with Tsallis thermodynamics [31–33], the particles measured in the experiment were produced by fireballs following the Tsallis distribution Eq. (1). The density distribution of these fireballs in the rapidity space is $\nu(y_f)$, where $y_f$ is the rapidity of the fireball. Therefore the transverse momentum spectrum of particles can be written as

$$\frac{d^2N}{2\pi p_T dp_T dy} = \frac{N}{A}\int_{-\infty}^{\infty}\nu\left(y_f\right)\frac{m_T\cosh\left(y-y_f\right)}{(2\pi)^3} \times\left[1+(q-1)\frac{m_T\cosh\left(y-y_f\right)}{T}\right]^{-\frac{q}{q-1}}dy_f, \quad (3)$$

where $N$ is the total particle multiplicity and $A$ is the normalization constant such that

$$\int_{-\infty}^{\infty}\int_0^{\infty}\frac{d^2N}{p_T dp_T dy}p_T dp_T dy = N. \quad (4)$$

Sometimes, the experimental data are measured in the pseudo-rapidity $\eta$ space. To describe the experimental data $\frac{dN}{d\eta}$, we substitute the relation between rapidity and pseudo-rapidity [36]

$$\frac{dy}{d\eta}(\eta,p_T) = \sqrt{1-\frac{m_0^2}{m_T^2\cosh^2 y}} \quad (5)$$

into Eq. (3) and integrate the transverse momentum in the equation to obtain [32, 33]

$$\frac{dN}{d\eta} = \frac{N}{A}\int_{-\infty}^{\infty}dy_f\int_0^{\infty}dp_T p_T\sqrt{1-\frac{m_0^2}{m_T^2\cosh^2 y}} \times\nu(y_f)\frac{m_T\cosh(y-y_f)}{(2\pi)^2} \times\left[1+(q-1)\frac{m_T\cosh(y-y_f)}{T}\right]^{-\frac{q}{q-1}}, \quad (6)$$

where

$$y=\frac{1}{2}\ln\left[\frac{\sqrt{p_T^2\cosh^2\eta+m_0^2}+p_T\sinh\eta}{\sqrt{p_T^2\cosh^2\eta+m_0^2}-p_T\sinh\eta}\right]. \quad (7)$$

Because of the term of $\sqrt{1-\frac{m_0^2}{m_T^2\cosh^2 y}}$, Eq. (6) cannot be analytically integrated over $p_T$ and it is done numerically.

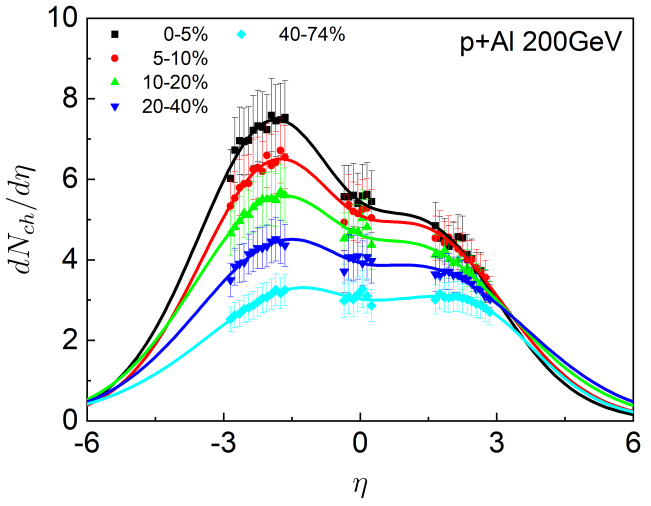


Fig. 1. (Color online) The pseudo-rapidity distributions of the charged particles produced in p+Al collisions at $\sqrt{s_{NN}}=200$ GeV for different centralities. The symbols are experimental data taken from [30]. The curves are the results from Eqs. (6) and (8).

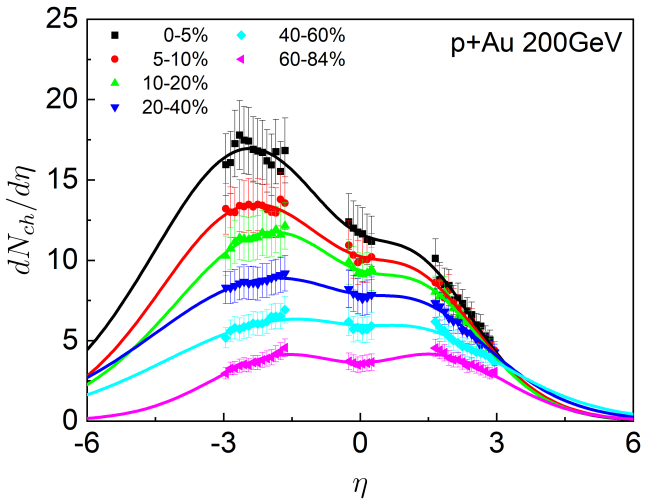


Fig. 2. (Color online) Same as Fig. 1, but for p+Au collisions at $\sqrt{s_{NN}}=200$ GeV.

In this paper the asymmetric collision systems are studied, so the distribution $\nu(y_f)$ is assumed to be the sum of two

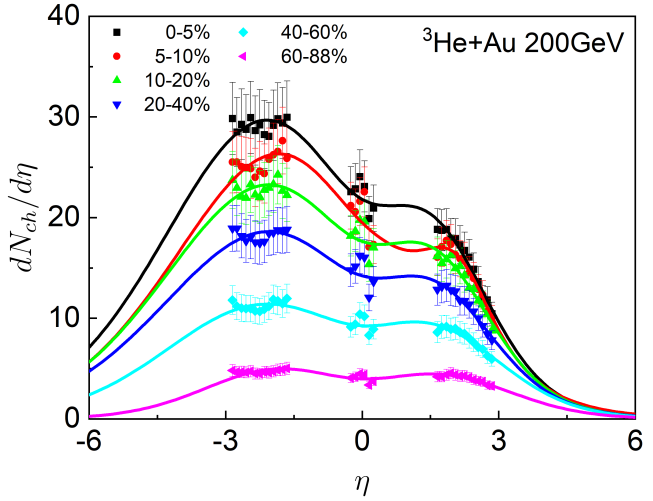


Fig. 3. (Color online) Same as Fig. 1, but for $^3$He+Au collisions at $\sqrt{s_{NN}} = 200$ GeV.

asymmetric $q$-Gaussian functions [33],

$$\nu\left(y_f\right) = \frac{1}{\sqrt{2\pi}\sigma_a}\left[1+\left(q'-1\right)\frac{\left(y_f-y_{0a}\right)^2}{2\sigma_a^2}\right]^{-\frac{1}{q'-1}} + \frac{x}{\sqrt{2\pi}\sigma_A}\left[1+\left(q'-1\right)\frac{\left(y_f+y_{0A}\right)^2}{2\sigma_A^2}\right]^{-\frac{1}{q'-1}}, \quad (8)$$

where $y_{0a(A)}$ and $\sigma_{a(A)}$ are the centroid position and width of fireball distribution in the direction of the light (heavy) nucleus beam, respectively. The normalization of Eq. (8) is handled by the normalization constant $A$ in Eq. (3). $x$ is the parameter to characterize the extent of asymmetry which was first proposed in our previous work [33]. In this work, we take $q' = q$ same as in [31–33]. A representative figure of Eq. (8) is shown in the Appendix A with the parameters obtained for the p+Al collisions at 0-5% centrality and $\sqrt{s_{NN}} = 200$ GeV.

## III. RESULTS AND DISCUSSION

Because the data of the transverse momentum spectra of the charged particles produced in p+Al, p+Au and $^3$He+Au collisions at $\sqrt{s_{NN}} = 200$ GeV have not been released yet, the data of the transverse momentum spectra of $\pi^0$ produced from these collisions are obtained from [37] in this study. Using Eq. (2) by taking $g = 1$ and V as a free parameter, the parameters $T$ and $q$ for the Tsallis distribution are extracted and listed in Table 2 in the Appendix B. A representative figure of transverse momentum spectra of $\pi^0$ for p+Al collisions at $\sqrt{s_{NN}} = 200$GeV is shown in Appendix C. It is worth noting that the transverse momentum spectrum of $\pi^0$ is very similar to that of $\pi^\pm$ at $\sqrt{s_{NN}} = 200$ GeV for a given collision centrality, the temperature parameter $T$ extracted from $\pi^0$ should reasonably characterize the property of the collision system. We take the parameters $T$ and $q$ from the closest centrality when the centrality of the particle transverse momentum spectrum and the centrality of the charged particle pseudorapidity distribution are not the same. These two parameters and the fireball model with Tsallis thermodynamics, Eqs. (6) and (8), are then utilized to study the pseudorapidity distribution of the charged particles produced in the collisions. The corresponding values of $x$ in Eq. (8) are also listed in Table 3 in the Appendix B.

In Figs. 1, 2 and 3 the results of the pseudo-rapidity distributions of the charged particles from the fireball model with Tsallis thermodynamics for different centrality bins in p+Al, p+Au and $^3$He+Au collisions at $\sqrt{s_{NN}} = 200$ GeV are shown. The fireball model effectively describes the experimental data within the errors. Notably, the data quality of the

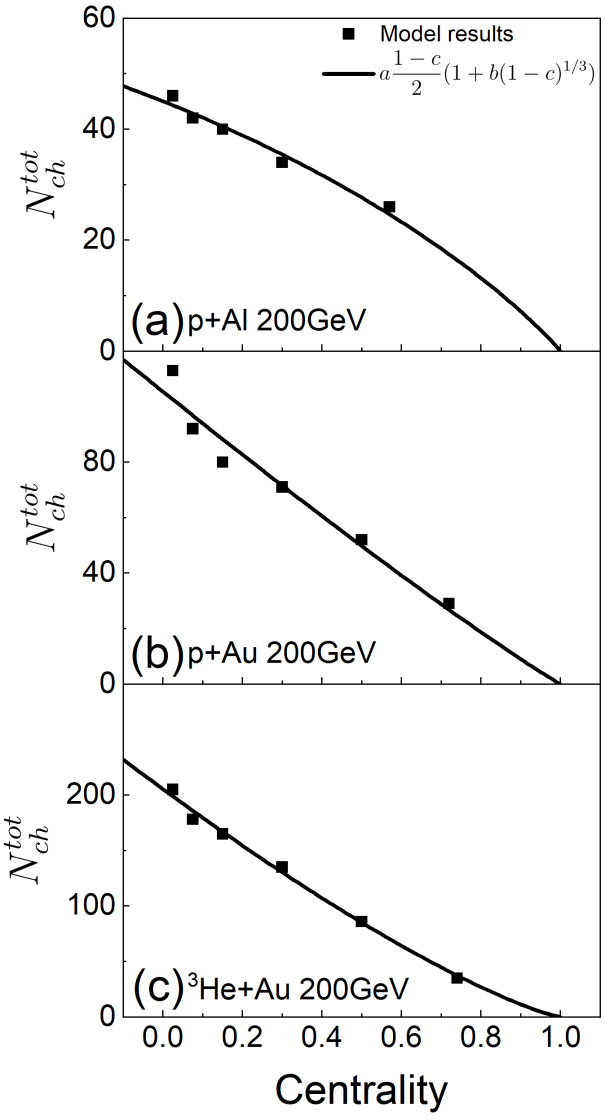


Fig. 4. Total charged particle multiplicities produced in the p+Al, p+Au and $^3$He+Au collisions at $\sqrt{s_{NN}} = 200$ GeV versus the collision centrality $c$. The squares are the fireball model results. The lines are the fitting results. The fitting function is from [14] and specified in the legend.

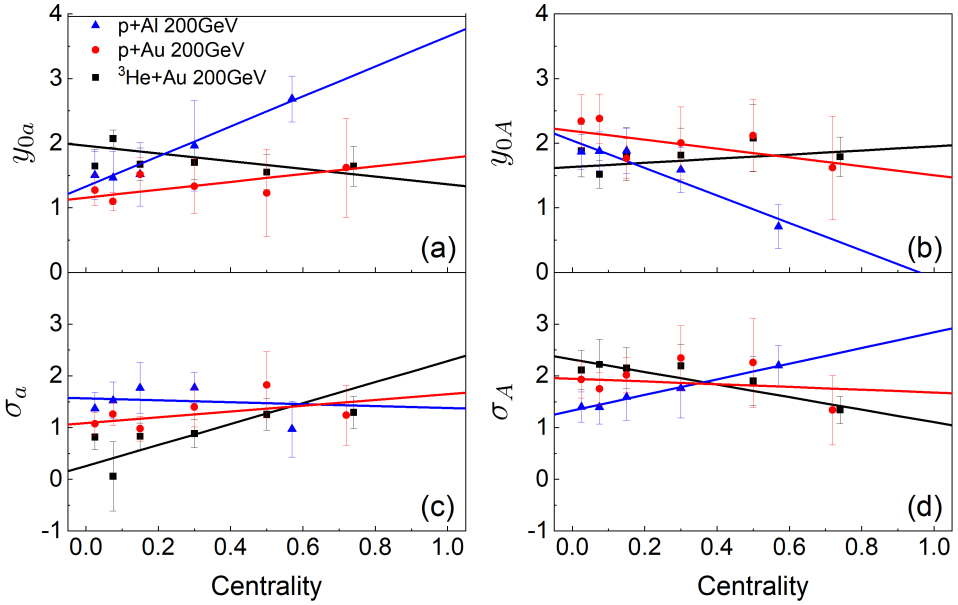


Fig. 5. (Color online) The centrality dependence of model parameters $y_{0a}$, $y_{0A}$, $\sigma_a$ and $\sigma_A$ in p+Al, p+Au and $^3$He+Au collision at $\sqrt{s_{NN}}$ = 200 GeV. The lines are the linear fit results to guide the eyes.

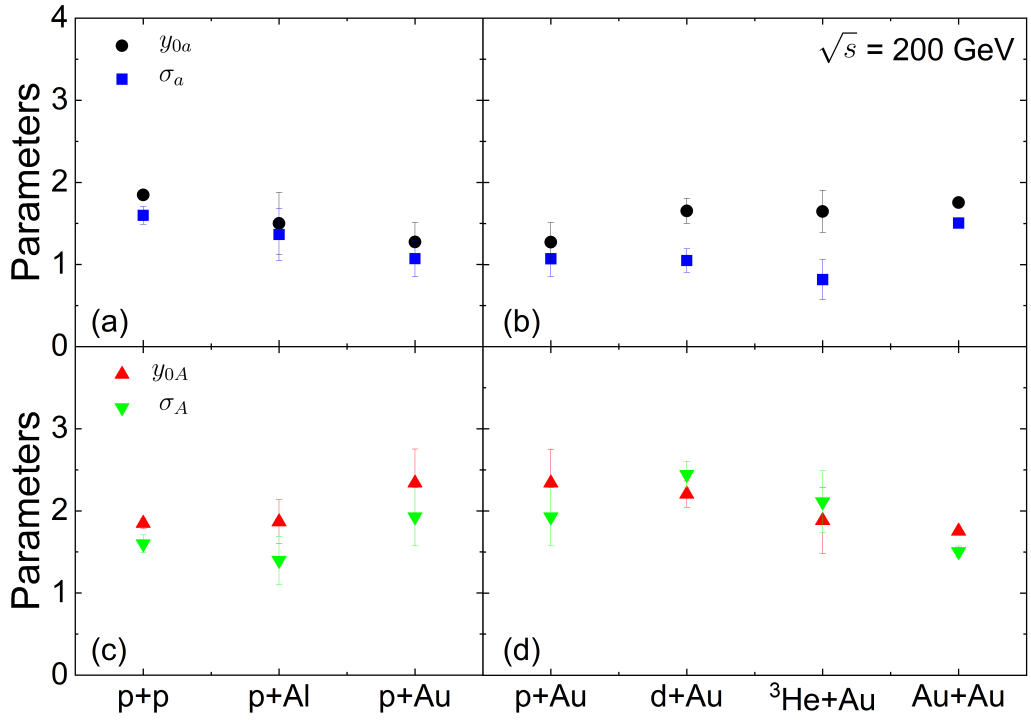


Fig. 6. (Color online) The collision system size dependence of model parameters $y_{0a}$, $y_{0A}$, $\sigma_a$, $\sigma_A$ for p+p, p+Al (0-5%), p+Au (0-5%), d+Au (0-20%), $^3$He+Au (0-5%) and Au+Au (0-6%) collisions at $\sqrt{s_{NN}}$ = 200 GeV. The parameters for the p+p, d+Au and Au+Au collisions are taken from Ref. [33].

pseudo-rapidity distributions of the charged particles is not as good as that for d+Au collisions at $\sqrt{s_{NN}}$ = 200 GeV shown in [33], i.e., in terms of larger errors, a fewer number of data points as well as a lower pseudo-rapidity coverage, which leads to larger uncertainties to the fireball model parameters and affects our analyses of the fireball model parameters versus collision centrality and collision system size to some extent later in the following. The pseudo-rapidity distribution of the charged particles for centrality 5-10% is lower than the case for centrality 10-20% in some pseudo-rapidity regions

for $^3$He+Au collisions which is observed in Fig. 3. A larger $x$ at centrality 5-10% compared with the others for $^3$He+Au collisions is also observed in Table 3. We emphasize that the same fitting protocol is applied for all the pseudo-rapidity distribution data of the charged particles. Because the collision system is asymmetric, the pseudo-rapidity distribution of the charged particles has significant forward/backward asymmetry. Fewer particles are produced in the direction of the light nucleus (p, $^3$He) beam compared to the heavy nucleus (Al, Au) beam. As the d+Au collision system at $\sqrt{s_{NN}} = 200$ GeV and the p+Pb collision system at $\sqrt{s_{NN}} = 5.02$ TeV we studied in [33], the pseudo-rapidity distributions of the charged particles produced by these collision systems also become more symmetric from the central to peripheral collisions. It is because the peripheral collisions for asymmetric collision systems are more similar to the symmetric p+p collisions according to collision geometry.

Table 1. Results of the linear fits are shown in Fig. 5. The c represents the centrality.

| System (GeV) | $y_{0a}$ | $\sigma_a$ | $y_{0A}$ | $\sigma_A$ |
|---|---|---|---|---|
| p+Al 200 | 2.32c+1.33 | -0.19c+1.57 | -2.13c+2.04 | 1.51c+1.32 |
| p+Au 200 | 0.61c+1.16 | 0.56c+1.09 | -0.69c+2.19 | -0.27c+1.95 |
| $^3$He+Au 200 | -0.60c+1.96 | 2.03c+0.26 | 0.32c+1.63 | -1.21c+2.32 |

We then evaluate the centrality dependence of the total multiplicities of the charged particles produced in these collision systems. Integrating Eq. (6) over the $\eta \in [-10, 10]$ we obtain the total multiplicity of the charged particles for each centrality from the fireball model. Because the corresponding experimental data are not yet available, we only analyze the results extracted from the fireball model and treat them as predictions. Figure 4 shows the total multiplicities of the charged particles calculated from the fireball model versus collision centrality $c$. $c = 0$ represents the most central collisions and $c = 1$ represents the most peripheral collisions. It can be observed that the fitting function taken from [14] can effectively describe the centrality dependence of the total multiplicities of the charged particles. As the centrality changes from the central to peripheral collisions, fewer charged particles are produced.

We also analyze both the centrality and system size dependence of the parameters ($y_{0a}$, $y_{0A}$, $\sigma_a$ and $\sigma_A$) of the fireball model. In Fig. 5 the dependence of the fireball model parameters on the collision centrality in the p+Al, p+Au and $^3$He+Au collisions at $\sqrt{s_{NN}} = 200$ GeV are shown. Inspired by the linear relation of the centrality dependence of the fireball model parameters for d+Au collisions at $\sqrt{s_{NN}} = 200$ GeV and p+Pb collisions at $\sqrt{s_{NN}} = 5.02$ TeV shown in Fig. 12 of our previous work [33], the linear fittings are performed to guide the eyes in Fig. 5 and the fitting functions are listed in Tab. 1. The negative and positive slopes of the linear fittings for the fireball model parameters ($y_{0a}, y_{0A}$ and $\sigma_A$) versus centrality are similar to those of the d+Au and p+Pb collisions in [33]. In the following discussion, the results for d+Au and p+Pb are obtained from [33]. It can be observed that the slopes of the linear fittings for parameter $y_{0a}$ versus centrality are positive and the corresponding slopes of the linear fittings for parameter $y_{0A}$ versus centrality are negative for p+Al, p+Au and d+Au collisions at $\sqrt{s_{NN}} = 200$ GeV. However, the slopes of the linear fittings for parameters $(y_{0a}, y_{0A})$ reverse the signs respectively for $^3$He+Au collision at $\sqrt{s_{NN}} = 200$ GeV compared to the above mentioned cases. The slopes of the linear fittings for parameters $(y_{0a}, y_{0A})$ are positive for p+Pb at $\sqrt{s_{NN}} = 5.02$ TeV. It can also be observed that there is a universal trend with increasing centrality for parameter $\sigma_{a(A)}$ except the lightest collision system p+Al, i.e., $\sigma_a$ increases with increasing centrality in the direction of the light nucleus beam and $\sigma_A$ decreases with increasing centrality in the direction of the heavy nucleus beam. In the p+Al collision system, $\sigma_a$ and $\sigma_A$ have opposite trends with increasing centrality to their counterparts in the other collision systems. These different patterns indicate the complex dynamics in the asymmetric collisions relevant to the combinations of the projectile and target as well as the collision energy which needs more investigations.

Figure 6 shows the collision system size dependence of the fireball model parameters at $\sqrt{s_{NN}} = 200$ GeV. For collision systems other than p+p, the parameters of the most central collisions are considered. In the p+p and Au+Au collisions, the parameters $y_{0a} = y_{0A} = y_0$, $\sigma_a = \sigma_A = \sigma$, where $y_0$ and $\sigma$ are the rapidity centroid and width of fireball distribution in the symmetric collision system, as detailed in [33]. It can be deduced that when the light nucleus is p, $y_{0a}$ decreases as the size of the heavy nucleus increases, whereas $y_{0A}$ shows the opposite trend. This indicates that a larger heavy nucleus has stronger stopping power for p. When the heavy nucleus is Au, $y_{0a}$ increases as the size of the light nucleus increases, whereas $y_{0A}$ shows the opposite trend. This means that a larger light nucleus is more difficult to be stopped by Au but has a stronger stopping power for Au. For parameters $\sigma_a$ and $\sigma_A$, no conclusive patterns are observed. We expect that more discussions can be added when the data quality of the pseudo-rapidity distributions of the charged particles is improved by experimentalists. These phenomena manifest the complex dynamics in the asymmetric collisions.

## IV. SUMMARY

In this paper, we studied the pseudo-rapidity distributions of the charged particles produced in p + Al, p + Au and $^3$He + Au collisions at $\sqrt{s_{NN}} = 200$ GeV using the fireball model with Tsallis thermodynamics. The model can well fit the experimental data from asymmetric collisions. We also extracted the total multiplicities of the charged particles from the fireball model as predictions and analyzed their dependence on collision centrality. Notably, the data quality of the pseudo-rapidity distributions of charged particles produced in p + Al, p + Au and $^3$He + Au collisions at $\sqrt{s_{NN}} = 200$ GeV affected our results to some extent. Combining our previous results of d+Au collisions at $\sqrt{s_{NN}} = 200$ GeV and p+Pb collision at $\sqrt{s_{NN}} = 5.02$ TeV, we analyzed the centrality and system size dependence of the fireball

model parameters ($y_{0a}$, $y_{0A}$, $\sigma_a$ and $\sigma_A$). Interesting patterns were revealed, which indicated the complex dynamics in the asymmetric collisions. Our results confirmed the conclusion made previously in [33] that the fireball model with Tsallis thermodynamics as a universal framework could also describe the pseudo-rapidity distribution of the charged particles produced in asymmetric collision systems.

**Author contributions** All authors contributed to the study conception and design. Material preparation, data collection and analysis were performed by Jun-Qi Tao, Hong-Bin He, Hua Zheng, Wen-Chao Zhang, Xing-Quan Liu, Li-lin Zhu and Aldo Bonasera. The first draft of the manuscript was written by Jun-Qi Tao and Hua Zheng and all authors commented on previous versions of the manuscript. All authors read and approved the final manuscript.

**Data Availability** The data that support the findings of this study are openly available in Science Data Bank at https://doi.org/10.57760/sciencedb.j00186.00293 and https://cstr.cn/31253.11.sciencedb.j00186.00293.



## Appendix A: Fireball distribution of Eq. (8)

A representative figure of the fireball distribution of Eq. (8) using the parameters obtained for the p+Al collisions at 0-5% centrality and $\sqrt{s_{NN}} = 200$ GeV is shown.

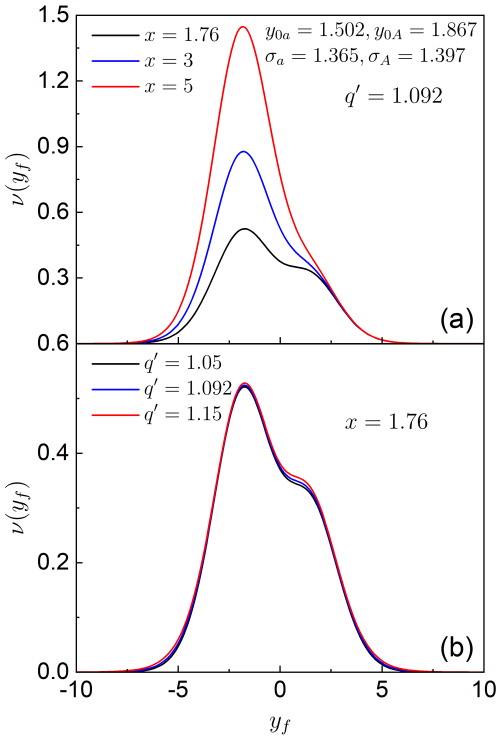


Fig. 7. (Color online) Fireball distribution with the parameters obtained from p+Al collisions for 0-5% centrality at $\sqrt{s_{NN}} = 200$ GeV is shown. (a) The value of $x$ is varied; (b) The value of $q'$ is varied.

## Appendix B: Parameters $q$, $T$ and $x$

The parameters of $q$ and $T$ extracted by fitting the transverse momentum spectrum of particles [37] with Tsallis distribution Eq. (2) as well as the parameter $x$ in Eq. (8) are listed.

Table 2. Parameters $q$ and $T$ for the p+Al, p+Au and $^3$He+Au collisions at $\sqrt{s_{NN}} = 200$ GeV for different centralities.

| System | Centrality | $q$ | $T$(GeV) | $\chi^2/NDF$ |
|---|---|---|---|---|
| p+Al | 0-5% | 1.092±0.004 | 0.127±0.012 | 0.129 |
| | 0-20% | 1.098±0.004 | 0.115±0.012 | 0.151 |
| | 20-40% | 1.101±0.004 | 0.107±0.010 | 0.288 |
| | 40-60% | 1.101±0.004 | 0.108±0.012 | 0.223 |
| | 60-72% | 1.103±0.005 | 0.098±0.013 | 0.232 |
| p+Au | 0-5% | 1.089±0.004 | 0.138±0.012 | 0.261 |
| | 0-20% | 1.090±0.004 | 0.138±0.012 | 0.117 |
| | 20-40% | 1.095±0.004 | 0.127±0.012 | 0.122 |
| | 40-60% | 1.096±0.004 | 0.123±0.012 | 0.204 |
| | 60-84% | 1.105±0.004 | 0.103±0.010 | 0.164 |
| $^3$He+Au | 0-5% | 1.092±0.004 | 0.133±0.010 | 0.082 |
| | 0-20% | 1.095±0.004 | 0.127±0.011 | 0.066 |
| | 20-40% | 1.098±0.004 | 0.118±0.011 | 0.046 |
| | 40-60% | 1.101±0.004 | 0.112±0.011 | 0.164 |
| | 60-84% | 1.103±0.004 | 0.104±0.011 | 0.157 |

Table 3. Parameter $x$ for the p+Al, p+Au and $^3$He+Au collisions at $\sqrt{s_{NN}} = 200$ GeV for different centralities.

| System | Centrality | $x$ |
|---|---|---|
| p+Al | 0-5% | 1.760±0.796 |
| | 5-10% | 1.313±0.620 |
| | 10-20% | 1.247±0.596 |
| | 20-40% | 1.430±0.840 |
| | 40-74% | 4.767±4.522 |
| p+Au | 0-5% | 4.098±1.540 |
| | 5-10% | 2.318±0.190 |
| | 10-20% | 4.690±1.637 |
| | 20-40% | 3.173±1.196 |
| | 40-60% | 1.470±0.194 |
| | 60-84% | 1.092±5.980 |
| $^3$He+Au | 0-5% | 5.912±1.926 |
| | 5-10% | 13.055±7.709 |
| | 10-20% | 5.470±1.900 |
| | 20-40% | 5.414±1.919 |
| | 40-60% | 2.210±0.957 |
| | 60-88% | 1.184±0.550 |

## Appendix C: The particle spectra fit

Using Eq. (2), the fitting figure of the transverse momentum spectra of $\pi^0$ produced in the p+Al collisions at $\sqrt{s_{NN}} = 200$ GeV is shown. Similar results are obtained for the p+Au and $^3$He+Au collision systems at $\sqrt{s_{NN}} = 200$ GeV.

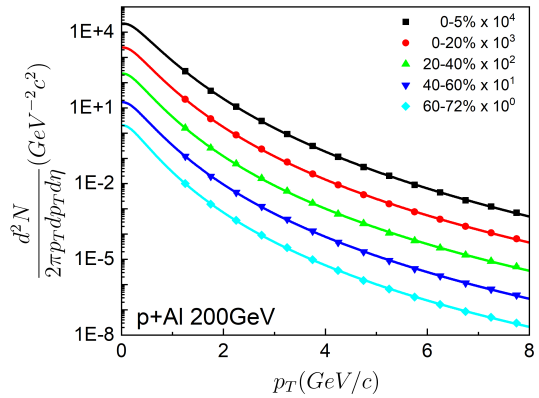


Fig. 8. (Color online) Transverse momentum spectra of $\pi^0$ produced in p+Al collisions at $\sqrt{s_{NN}} = 200$ GeV [37]. The curves are the corresponding fittings using Eq. (2).

[1] X. N. Wang, M. Gyulassy, HIJING: A Monte Carlo model for multiple jet production in pp, pA, and AA collisions. Phys. Rev. D, **44**, 3501 (1991). doi: 10.1103/PhysRevD.44.3501

[2] Z. W. Lin, C. M. Ko, B. A. Li, B. Zhang, S. Pal, Multiphase transport model for relativistic heavy ion collisions. Phys. Rev. C, **72**, 064901 (2005). doi: 10.1103/PhysRevC.72.064901

[3] H. Wang, J. H. Chen, Y. G. Ma, S. Zhang, Charm hadron azimuthal angular correlations in Au + Au collisions at $\sqrt{s_{NN}}$ = 200 GeV from parton scatterings. NST, **30**, 185 (2019). doi: 10.1007/s41365-019-0706-z

[4] Z. W. Lin, L. Zheng, Further developments of a multi-phase transport model for relativistic nuclear collisions. NST, **32**, 113 (2021). doi: 10.1007/s41365-021-00944-5

[5] T. Pierog, Iu. Karpenko, J. M. Katzy, E. Yatsenko, K. Werner, EPOS LHC: Test of collective hadronization with data measured at the CERN Large Hadron Collider. Phys. Rev. C, **92**, 034906 (2015). doi: 10.1103/PhysRevC.92.034906

[6] X. J. Sun, C. X. Tian, E. Q. Wang, F. H. Liu, Dependence of Charged Particle Pseudorapidity Distributions on Centrality in Pb—Pb Collisions at $\sqrt{s_{NN}}$ = 2.76 TeV. Chinese Phys. Lett., **30**, 022501 (2013). doi: 10.1088/0256-307X/30/2/022501

[7] B. C. Li, Y. Z. Wang, F. H. Liu, X. J. Wen, Y. E. Dong, Particle production in relativistic $pp(\overline{p})$ and $AA$ collisions at RHIC and LHC energies with Tsallis statistics using the two-cylindrical multisource thermal model. Phys. Rev. D, **89**, 054014 (2014). doi: 10.1103/PhysRevD.89.054014

[8] L. N. Gao, F. H. Liu, On Pseudorapidity Distribution and Speed of Sound in High Energy Heavy Ion Collisions Based on a New Revised Landau Hydrodynamic Model. Adv. High Energy Phys., 184713 (2015). doi: 10.1155/2015/184713

[9] Z. J. Jiang, D. F. Xu, Y. Huang, A Description of Pseudorapidity Distributions of Charged Particles Produced in Au+Au Collisions at RHIC Energies. Adv. High Energy Phys., 1369098 (2018). doi: 10.1155/2018/1369098

[10] Z. J. Jiang, H. P. Deng, Y. Huang, A Universal Description of Pseudorapidity Distributions in Both Nucleus-Nucleus and p-p Collisions at Currently Available Energies. Adv. High Energy Phys., 5308084 (2016). doi: 10.1155/2016/5308084

[11] W. B. Zhao, S. Ryu, C. Shen, B. Schenke, 3D structure of anisotropic flow in small collision systems at energies available at the BNL Relativistic Heavy Ion Collider. Phys. Rev. C, **107**, 014904 (2023). doi: 10.1103/PhysRevC.107.014904

[12] E. Abbas, et al., (ALICE Collaboration), Centrality dependence of the pseudorapidity density distribution for charged particles in Pb–Pb collisions at $\sqrt{s_{NN}}$ = 2.76 TeV. Phys. Lett. B, **726**, 610 (2013). doi: 10.1016/j.physletb.2013.09.022

[13] J. Adam, et al., (ALICE Collaboration), Centrality evolution of the charged-particle pseudorapidity density over a broad pseudorapidity range in Pb-Pb collisions at $\sqrt{s_{NN}}$ = 2.76 TeV. Phys. Lett. B, **754**, 373 (2016). doi: 10.1016/j.physletb.2015.12.082

[14] J. Adam, et al., (ALICE Collaboration), Centrality dependence of the pseudorapidity density distribution for charged particles in Pb–Pb collisions at $\sqrt{s_{NN}}$ = 5.02 TeV. Phys. Lett. B, **772**, 567 (2016). doi: 10.1016/j.physletb.2017.07.017

[15] S. Acharya, et al., (ALICE Collaboration), Centrality and pseudorapidity dependence of the charged-particle multiplicity density in Xe–Xe collisions at $\sqrt{s_{NN}}$ = 5.44 TeV. Phys. Lett. B, **790**, 35 (2019). doi: 10.1016/j.physletb.2018.12.048

[16] G. J. Alner, et al., (UA5 Collaboration), Scaling of pseudorapidity distributions at c.m. energies up to 0.9 TeV. Z. Phys. C, **33**, 1 (1986). doi: 10.1007/BF01410446

[17] B. Alver, et al., (PHOBOS Collaboration), Charged-particle multiplicity and pseudorapidity distributions measured with the PHOBOS detector in Au + Au, Cu + Cu, d + Au, and p + p collisions at ultrarelativistic energies. Phys. Rev. C, **83**, 024913 (2011). doi: 10.1103/PhysRevC.83.024913

[18] K. Aamodt, et al., (ALICE Collaboration), Charged-particle multiplicity measurement in proton–proton collisions at $\sqrt{s_{NN}}$ = 0.9 and 2.36 TeV with ALICE at LHC. Eur. Phys. J. C, **68**, 89 (2010). doi: 10.1140/epjc/s10052-010-1339-x

[19] J. Adam, et al., (ALICE Collaboration), Charged-particle multiplicities in proton–proton collisions at $\sqrt{s_{NN}}$ = 0.9 to 8 TeV. Eur. Phys. J. C, **77**, 33 (2017). doi: 10.1140/epjc/s10052-016-4571-1

[20] J. Adam, et al., (ALICE Collaboration), Pseudorapidity and transverse-momentum distributions of charged particles in proton–proton collisions at $\sqrt{s_{NN}}$ = 13 TeV. Phys. Lett. B, **753**, 319 (2016). doi: 10.1016/j.physletb.2015.12.030

[21] F. Abe, et al., (CDF Collaboration), Pseudorapidity distributions of charged particles produced in $\overline{p}p$ interactions as $\sqrt{s}$ = 630 and 1800 GeV. Phys. Rev. D, **41**, 2330 (1990). doi: 10.1103/PhysRevD.41.2330

[22] G. Arnison, et al., (UA1 Collaboration), Charged particle multiplicity distributions in proton-antiproton collisions at 540 GeV centre of mass energy. Phys. Lett. B, **123**, 108 (1983). doi: 10.1016/0370-2693(83)90969-3

[23] W. Thome, et al., (Aachen-CERN-Heidelberg-Munich Collaboration), Charged particle multiplicity distributions in pp collisions at ISR energies. Nucl. Phys. B, **129**, 365 (1977). doi: 10.1016/0550-3213(77)90122-5

[24] B. B. Back, et al., (PHOBOS Collaboration), Significance of the Fragmentation Region in Ultrarelativistic Heavy-Ion Collisions. Phys. Rev. Lett., **91**, 052303 (2003). doi: 10.1103/PhysRevLett.91.052303

[25] B. Alver, et al., (PHOBOS Collaboration), System Size, Energy, and Centrality Dependence of Pseudorapidity Distributions of Charged Particles in Relativistic Heavy-Ion Collisions. Phys. Rev. Lett. **102**, 142301 (2007). doi: 10.1103/PhysRevLett.102.142301

[26] B. B. Back, et al., (PHOBOS Collaboration), Charged-particle pseudorapidity distributions in Au+Au collisions at $\sqrt{s_{NN}}$ = 64 GeV. Phys. Rev. C, **74**, 021901(R) (2005). doi: 10.1103/PhysRevC.74.021901

[27] B. B. Back, et al., (PHOBOS Collaboration), Scaling of charged particle production in d + Au collisions at $\sqrt{s_{NN}}$ = 200 GeV. Phys. Rev. C, **72**, 031901(R) (2005). doi: 10.1103/PhysRevC.72.031901

[28] G. Aad, et al., (ATALS Collaboration), Measurement of the centrality dependence of the charged-particle pseudorapidity distribution in proton–lead collisions at $\sqrt{s_{NN}}$ = 5.02 TeV with the ATLAS detector. Eur. Phys. J. C, **76**, 199 (2016). doi: 10.1140/epjc/s10052-016-4002-3

[29] V. Khachatryan, et al., (CMS Collaboration), Transverse-momentum and pseudorapidity distributions of charged hadrons in pp collisions at $\sqrt{s_{NN}}$ = 0.9 and 2.36 TeV. J. High Energ. Phys., **2010**, 41 (2010). doi: 10.1007/JHEP02(2010)041

[30] A. Adare, et al., (PHENIX Collaboration), Pseudorapidity Dependence of Particle Production and Elliptic Flow in Asymmetric Nuclear Collisions of p + Al, p + Au, and $^3$He + Au at $\sqrt{s_{NN}}$ = 200 GeV. Phys. Rev. Lett., **121**, 222301 (2018). doi: 10.1103/PhysRevLett.121.222301

[31] L. Marques, J. Cleymans, A. Deppman, Description of high-energy pp collisions using Tsallis thermodynamics: Transverse momentum and rapidity distributions. Phys. Rev. D **91**, 054025 (2015). doi: 10.1103/PhysRevD.91.054025

[32] Y. Gao, H. Zheng, L. L. Zhu, A. Bonasera, Description of charged particle pseudorapidity distributions in Pb+Pb collisions with Tsallis thermodynamics. Eur. Phys. J. A, **53**, 197

(2017). doi: 10.1140/epja/i2017-12397-y

[33] J. Q. Tao, M. Wang, H. Zheng, W. C. Zhang, L. L. Zhu, A. Bonasera, Pseudorapidity distributions of charged particles in pp($\overline{\text{p}}$), p(d)A and AA collisions using Tsallis thermodynamics. J. Phys. G, **48**, 105102 (2021). doi: 10.1088/1361-6471/ac1393

[34] C. Tsallis, Possible Generalization of Boltzmann-Gibbs Statistics. J. Stat. Phys., **52**, 479 (1988). doi: org/10.1007/BF01016429

[35] G. Wilk, Z. Włodarczyk, Consequences of temperature fluctuations in observables measured in high-energy collisions. Eur. Phys. J. A, **48**, 161 (2012). doi: org/10.1140/epja/i2012-12161-y

[36] C. Y. Wong, *Introduction to High-Energy Heavy-Ion Collisions*. (Singapore, World Scientific, 1994)

[37] U. A. Acharya, et al., (PHENIX Collaboration), Systematic study of nuclear effects in p + Al, p + Au, d + Au, and $^3$He + Au collision at $\sqrt{s_{NN}}$ = 200 GeV using $\pi^0$ production. Phys. Rev. C, **105**, 064902 (2022). doi: 10.1103/PhysRevC.105.064902